EFFECTS OF COHERENCE AND DOMAIN WALLS ON DIFFRACTION PROFILES IN RARE-EARTH DOPED $PbTiO_3$.

EFECTOS DE LA COHERENCIA Y LAS PAREDES DE DOMINIO EN LOS PERFILES DE DIFRACCIÓN EN $PbTiO_3$ DOPADO CON TIERRAS RARAS.

D. Camejo-González[a], A. Pentón-Madrigal[a,b†], A. Peláiz-Barranco[c]

a) Facultad de Física, Universidad de la Habana, San Lázaro y L. CP 10400. La Habana. Cuba. arbelio@fisica.uh.cu†
b) Instituto de Ciencias y Tecnología de Materiales, Universidad de la Habana (IMRE).
c) Grupo de Materiales Ferroicos, Facultad de Física, Universidad de la Habana. San Lázaro y L, Vedado. La Habana 10400, Cuba.
† corresponding author

Recibido 12/9/2025; Aceptado 15/11/2025

The paper presents a study concerning the coherence and domain wall effects on the profile of selected X-ray diffraction (XRD) peaks from the ferroelectric system $Pb_{0.92}Ln_{0.08}TiO_3$ (Ln^{3+} = La^{3+}, Dy^{3+}). The analysis focuses on the *hkl*-dependent broadening and asymmetry of certain diffraction peaks. The study was conducted using a diffraction model evaluated with experimentally determined parameters from XRD and Transmission Electron Microscopy (TEM). The results show that both coherence effects and domain wall scattering contribute significantly to peak asymmetries and diffuse intensity between (*h00*)/(*00h*) doublets. The results also show that these effects are sensitive to domain size being more pronounced in lower-order reflections. The choice of dopant directly impacts microstructural parameters. The study highlights the complexity of quantifying ferroelectric microstructures alone from diffraction data.

El artículo presenta un estudio sobre los efectos de coherencia y de pared de dominio en el perfil de determinados máximos de difracción de rayos X (DRX) del sistema ferroeléctrico $Pb_{0.92}Ln_{0.08}TiO_3$ (Ln^{3+} = La^{3+}, Dy^{3+}). El análisis se centra en el ensanchamiento y la asimetría dependientes de *hkl* de ciertos picos de difracción. El estudio se realizó utilizando un modelo de difracción evaluado con parámetros determinados experimentalmente mediante DRX y microscopía electrónica de transmisión. Los resultados muestran que tanto los efectos de coherencia como la dispersión de pared de dominio contribuyen significativamente a las asimetrías de los picos y a la intensidad difusa entre los dobletes (*h00*)/(*00h*). Los resultados también muestran que estos efectos son sensibles al tamaño del dominio y es más pronunciado en reflexiones de orden inferior. La elección del dopante afecta directamente a los parámetros microestructurales. El estudio destaca la complejidad de cuantificar las microestructuras ferroeléctricas únicamente a partir de datos de difracción.

Keywords: X-ray diffraction (Difracción de rayos X), microstructure (Microestructura), crystal defects (Defectos cristalinos), Fourier analysis (Análisis de Fourier), ferroelectric materials (Materiales ferroeléctricos).

I. INTRODUCTION

Ferroelectric ceramics based on lead titanate ($PbTiO_3$) are characterized by a domain structure that dictates their functional performance [1]. A critical aspect of microstructural characterization is understanding the contributions of various defects to X-ray diffraction (XRD) profiles, which are commonly used to determine microstructural parameters. In materials with 90° domain walls, such as tetragonal ferroelectrics, the analysis is complicated by anisotropic peak broadening, asymmetry, and diffuse scattering between fundamental reflections like the (*00h*)/(*h00*) doublet [2–9].

While domain walls are often cited as the primary source of these features, the role of coherence effects - the constructive and destructive interference of X-rays between adjacent crystalline domains - is frequently overlooked. Subsequent studies have further emphasized the importance of accounting for these effects in materials with complex domain structures [9–13]. This work presents an analysis of these contributions in rare-earth doped PbLnTiO (Ln^{3+} = La^{3+}, Dy^{3+}). Lead titanate (PT) ferroelectric system exhibits a high tetragonality, which promotes microstructural strains when the temperature changes around the Curie temperature and prevents the sintering of high density ceramic materials. Therefore, the study of lanthanide doping (PT) has attracted increasing attention, providing a lower tetragonality while good piezoelectric and ferroelectric properties are retained [14, 15].

A simple diffraction model [9] allows evaluating numerically both coherence and domain wall effects contributions to the diffracted intensity distribution from two neighboring domains. Boysen's model approaches the diffraction problem as a stacking of ordered atomic planes, where domain boundaries act as stacking faults (twins). In [9] it is demonstrates, through calculated examples, how these effects modify the intensity distribution in specific crystalline systems. Intensity distributions are generated for a given number of atomic layers within the ferroelectric domain, based on a specific selection criterion. The resulting data is then compared with experimental intensity distributions. In contrast, this manuscript explores the possibility of directly determining the average number of atomic layers within the domain from high-resolution XRD and TEM experiments to evaluate the model and thus estimate the coherence and

domain wall effects on the observed intensity distribution.

II. THE DIFFRACTION MODEL

From the Boysen model, expressions (1) and (2) can be obtained, which are key to the diffracted intensity distribution [9]. Equation (1) describes the diffracted intensity for two neighboring ferroelectric domains separated by an infinitely thin domain wall:quiero algo asi

$$I = 1 + S_1^2 + S_2^2 + S_{coh} \tag{1}$$

with

$$S_1 = \frac{\sin(\pi N(\Delta_x\xi + \Delta_v\eta))}{\sin(\pi(\Delta_x\xi + \Delta_v\eta))} \text{ and } S_2 = \frac{\sin(\pi N(\Delta_x\xi - \Delta_v\eta))}{\sin(\pi(\Delta_x\xi - \Delta_v\eta))} \tag{1a}$$

where S_1^2 and S_2^2 represent the intensities from each domain separately, and the constant 1 in (1) is the contribution from the domain wall. The coherent term S_{coh} (interference term in [9]) is given by:

$$S_{coh}(h) = 2\gamma\left(\frac{\sin(\beta(h + rk))}{\sin(\pi(h + rk))} \cdot \frac{\sin(\beta(h - rk))}{\sin(\pi(h - rk))}\right) \tag{1b}$$

where $\gamma = \cos(2\pi Nh - 1)$ and $\beta = \pi(N + 1)$.

In equation (1a) Δ_x represents a constant spacing of atomic planes parallel to the infinitely thin domain wall; Δ_v represents a constant lateral shift of such planes respect each other perpendicular to the stacking direction (see Fig. 1a in [9]). The quantities ξ and η are defined in reciprocal units. In both, (1a) and (1b), N can be assumed as the average number of atomic planes in each domain.

In equation (1b) the Miller indices h and k are defined with respect to a cubic crystallographic basis, where h takes continuous values and k takes integer values. The quantity r is related to the strain defined as:

$$r = \frac{1 + e}{2}, \quad \text{with} \quad e = \frac{\Delta_v - \Delta_x}{\Delta_x}.$$

On the other hand, equation (2) incorporates the finite width of the domain wall into the diffracted intensity distribution:

$$F(h) = \sum_{n=-N}^{N} \exp\left[2\pi i\left(nh + \frac{\Delta_x}{\Delta_y}\left[\pm n + e_o \cdot n_w \cdot \ln\left[\cosh\left(\frac{n}{n_w}\right)\right]\right]k\right)\right] \tag{2}$$

where $W = n_w\Delta_x$ is the width of the wall expressed in units of Δ_x . Equations (1) and (2) can be evaluated numerically as a function of N for integer values of k over a given range of h. The remaining parameters in (1) and (2) are determined by the lattice parameters of the crystal system.

To analyze the contribution of coherence effects and domain walls to the intensity distribution, the average coherent domain size is defined as [9]:

$$\langle L\rangle = N\Delta x \tag{3}$$

where $\langle L\rangle$ represents the average coherent domain size. This quantity can be determined directly from peak profiles analysis of the diffraction maxima. Given $\langle L\rangle$, N is calculated from equation (3).

III. EXPERIMENTAL PROCEDURE

The $Pb_{0.88}La_{0.08}TiO_3$ (PTLa8) and $Pb_{0.88}Dy_{0.08}TiO_3$ (PTDy8) ceramics were synthesized via the conventional ceramic method [16]. Both compositions were selected from a wide lanthanide series considering their significantly different properties (e.g., spontaneous polarization) and degrees of tetragonality [13].

High-resolution XRD experiments were carried out at the XPD line at LNLS, Campinas, Brazil. A Hubber diffractometer with Bragg-Brentano geometry was equipped with a Si(111) monochromator crystal and a Ge(111) analyzer crystal, using a wavelength of 1.77093 Å. Powder samples were mounted on a rotating sample holder to improve measurement statistics. Data were collected at room temperature from 20° to 98° with a step size of 0.02°. A LaB_6 standard was measured to account for the instrumental contribution to peak profile.

Transmission electron microscopy (TEM) was conducted at 200 kV on one JEM- 2100 TEM, Jeol). Samples for TEM were prepared by a mechanical process (Disc grinder Mod. 623 and Dimple Grinder Mod. 656, Gatan) followed by Ar ion milling (PIPS 691, Gatan).

IV. EVALUATING COHERENCE AND DOMAIN WALL EFFECTS BY USING EXPERIMENTAL DATA FOR PTLa8 AND PDy8 CERAMICS

The average coherent domain size and unit cell parameters were determined from high-resolution XRD patterns in order to evaluate equations (1) and (2). Figure 1 shows the selected reflections for the analysis, the (001)/(100) and (002)/(200) doublets for each system. They allows analysis along two mutually perpendicular crystallographic directions: [001] and [100], including reflections of different orders. The (h00) and (00h) peaks exhibit details that vary with the rare-earth element. Anisotropic broadening is observed, ie. the integral width for the (00h) peaks is greater than that of the (h00) peaks. The diffuse intensity between the doublets, resulting in asymmetry, is typically associated with 90° domain wall effects [2, 6–9]. The (00h) peaks are asymmetric on the right side, while the (h00) peaks are asymmetric on the left side. Peaks of the form (hhh) show no asymmetry. These anisotropic broadening and asymmetry effects are more pronounced in the PTLa8 sample.

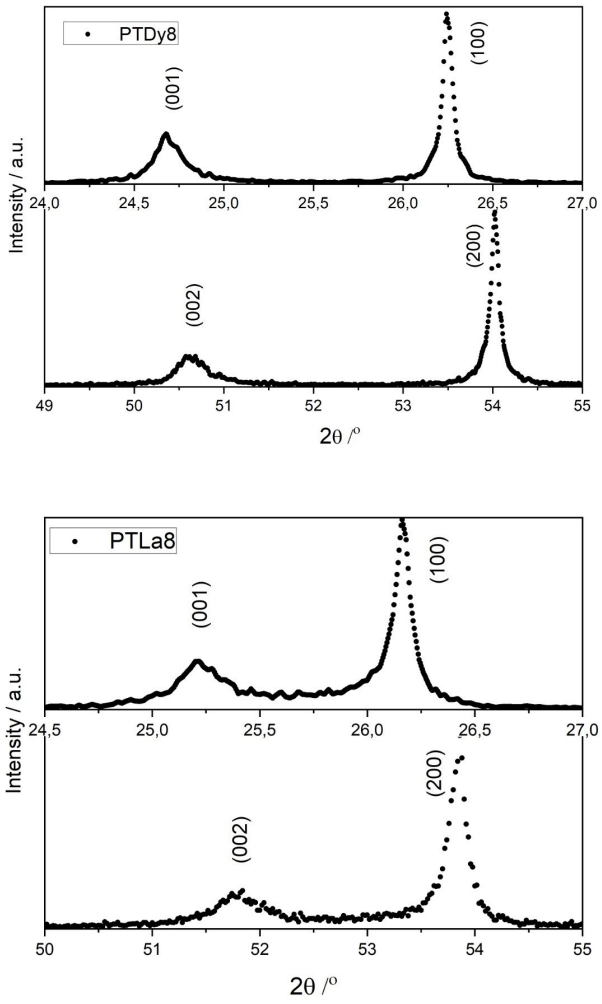

Figure 1. Peak shapes for PTDy8 and PTLa8, where (00*h*) peaks exhibit asymmetry on the right side of the profile while the (*h*00) peaks exhibit it on the left side.

The Warren-Averbach (WA) method [17] was applied, by using Fourier analysis, to investigate the ferroelectric microstructure. Reflections of different orders were selected to separate contributions from coherent domain size and non-uniform microstrains to the diffraction profiles. The selected (001)/(002) and (100)/(200) doublets satisfy the requirement of nonoverlapping with neighboring reflections, though care was taken with PTLa8 due to partial overlap in the internal region of the doublets (Fig. 1).

Following [6], the symmetric and asymmetric components of the doublets were separated. The left side of the (00*h*) profiles and the right side of the (*h*00) profiles were fitted using a split pseudoVoigt (pVwith) function, accounting for background. Symmetric profiles were simulated using pV functions based on the fitted parameters from each side, and the asymmetric components were obtained by subtracting these symmetric profiles from the experimental data.

Figure 2 shows the normalized experimental peaks (black points) and the calculated symmetric profiles (solid red curves) for the (002)/(200) doublet. The difference curves (bottom) represent the asymmetric components between the maxima positions $2\theta^{(002)}_{max}$ and $2\theta^{(200)}_{max}$. As referenced above, the asymmetric components are attributed to diffuse scattering from the 90° domain walls, while the symmetric components can be associated with the ferroelectric domains. After obtaining the symmetric profiles, the instrumental contribution was removed using a LaB_6 standard.

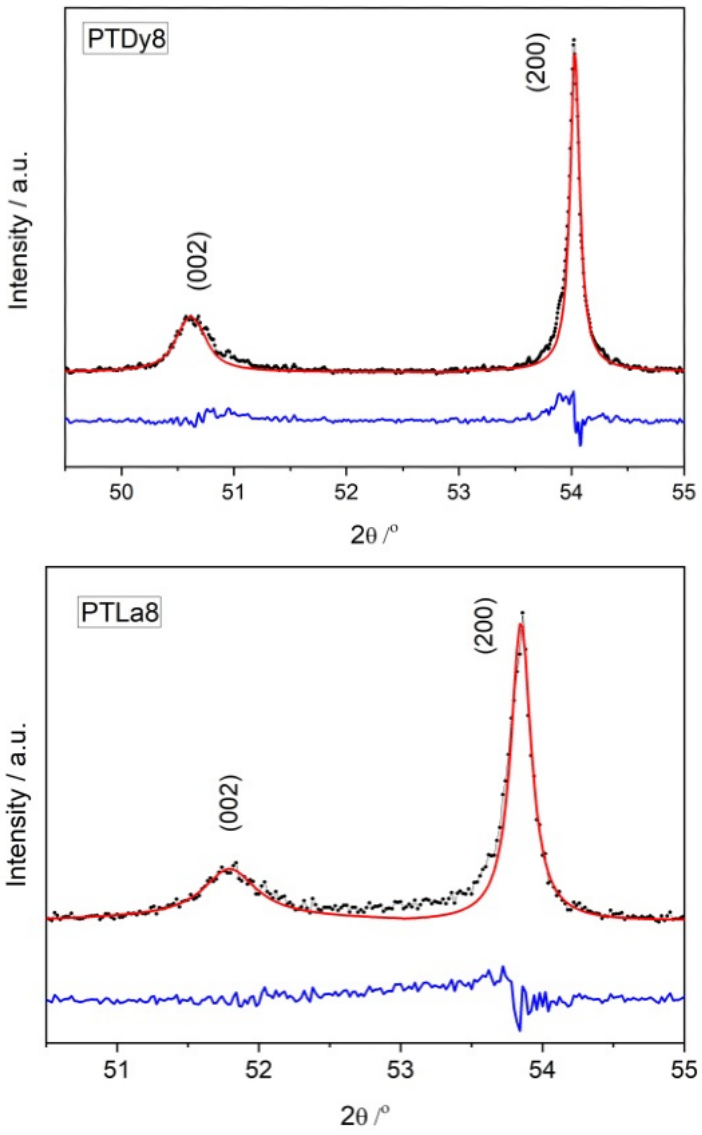

Figure 2. Experimental peaks (black), symmetric peaks (red) and the curve difference between them (blue) are shown for the (002)/(200) doublet of each sample.

IV.1. Symmetric components of the (00h)/(h00) doublets.

Two pairs of intrinsic symmetric reflections of different orders allowed the application of the WA method along the [001] and [100] directions. Assuming that crystal defects other than domain walls do not significantly affect the peak width, the calculated coherent domain size $\langle L \rangle$ can be considered a good approximation of the ferroelectric domain size and shape.

Figure 3 shows calculated Fourier coefficients (A_L^S) for

[001] and [100] directions. As stated by the WA method, the intercept of the initial slope of each curve with the abscissa axis (e.g. red dotted line) represents the average value of coherent domain size $\langle L \rangle$ and it can be assumed as the average ferroelectric domains sizes along the two considered crystallographic directions.

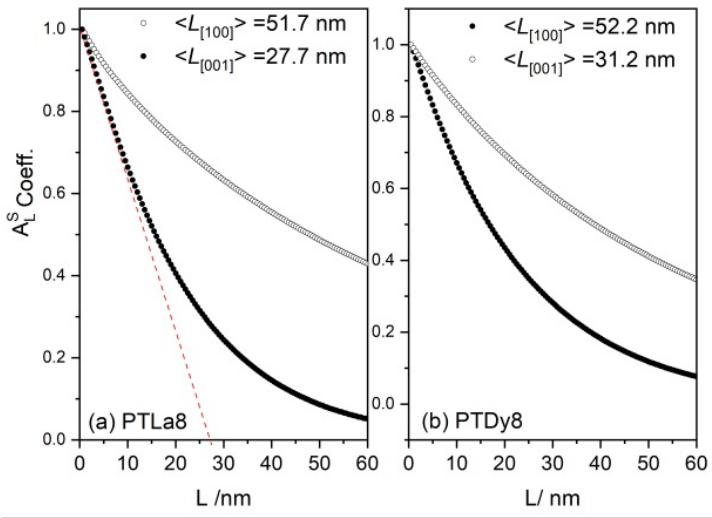

Figure 3. Fourier coefficients A_L^S for multi-order reflections and the corresponding $\langle L \rangle$ values along the [100] and [001] crystallographic directions for (a) PTLa8 and (b) PTDy8.

The average number of atomic layers per domain $\langle N \rangle$, was calculated using equation (3) by the computed values of $\langle L \rangle$ and Δ_x . Referring to Fig. 1a in [9], the quantities Δ_x and Δ_y have been redefined for the purpose of the present study and they can now be expressed in terms of: $\langle L \rangle_{[100]}$ and $\langle L \rangle_{[001]}$ as:

$$\Delta_y^* = \sqrt{(\langle L \rangle_{[100]})^2 + (\langle L \rangle_{[001]})^2} \tag{4a}$$

$$\Delta_x^* = \frac{(\langle L \rangle_{[100]})(\langle L \rangle_{[001]})}{\Delta_y^*} \tag{4b}$$

The average number of layers in each domain can be estimated as:

$$\langle N \rangle = \frac{\Delta_x^*}{\Delta_x} \tag{5}$$

Table 1 summarizes the unit cell and microstructural parameters for each sample along the [100] and [001] directions.

Parameter	Sample	
	PTDy8	PTLa8
a / Å	3.8989 ± 4E−4	3.9112 ± 9E−4
c / Å	4.1398 ± 6E−4	4.0529 ± 1E−4
$\langle L \rangle_{[100]}$ / nm	52.2 ± 0.1	51.7 ± 0.2
$\langle L \rangle_{[001]}$ / nm	31.2 ± 0.2	27.7 ± 0.2
$\langle L \rangle$ / nm	26.8 ± 0.2	24.4 ± 0.2
$\langle N \rangle$	94 ± 1	86 ± 1

Table 1. Sample parameters for PTDy8 and PTLa8.

The results indicate that ferroelectric domains are elongated nano-regions along the [100] direction and narrower along the [001] direction within the grains. This lamellar microstructure has been reported in other ferroelectric ceramic systems [18]. The nano-sized domains suggest that (Pb, Ln)TiO_3 develops a high density of domain walls (twinned crystals). Doping affects the average domain size, which decreases with decreasing ionic radius, particularly along [001]. This can be interpreted as an increase in 90° domain wall density.

The XRD results agree with TEM experiments. TEM micrographs of PTLa8 (Fig. 4) reveal a dense distribution of 90° domain walls with the described lamellar morphology. Suitable TEM samples for PTDy8 could not be prepared.

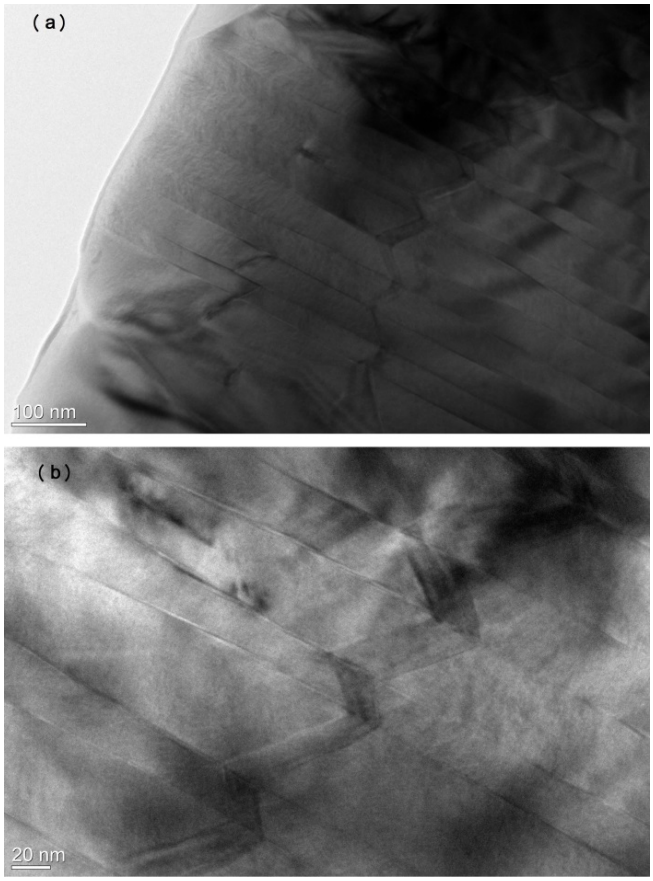

Figure 4. TEM micrograph of the PTLa8 sample showing (a) contrast due to high density of twining within a grain, (b) magnification of the same area revealing details of domain walls.

Using the calculated $\langle N \rangle$ values (Table 1), equation (1) can be evaluated numerically in the reciprocal space. The coherence effect on the diffracted intensity from two neighboring domains is represented for any of the peaks of the doublet. Figures 5 and 6 show the intensity distribution for $k = 1$ and $k = 2$ for both $\langle N \rangle$ values. The top panels show the coherence term (S_{coh}), and the bottom panels show the total intensity distribution.

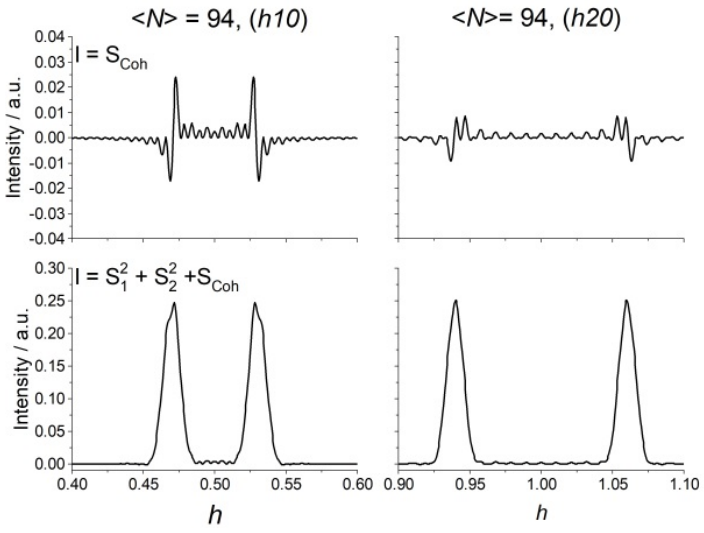

Figure 5. Coherence effect between neighboring domains for $\langle N \rangle = 94$ with $k = 1$ and $k = 2$. Top panel shows the S_{coh} term; bottom panel shows the total diffracted intensity.

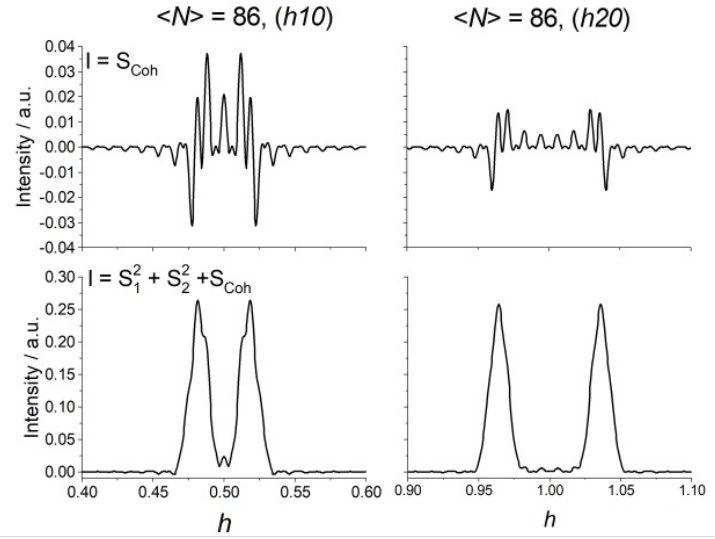

Figure 6. Coherence effect between neighboring domains for $\langle N \rangle = 86$ with $k = 1$ and $k = 2$. Top panel shows the S_{coh} term; bottom panel shows the total diffracted intensity.

Some conclusions can be drawn from the above results. Coherence effects are sensitive to $\langle N \rangle$ ($\langle L \rangle$). For $\langle N \rangle = 94$, the contribution to the total diffracted intensity is approximately 7 % for $k = 1$ and 4 % for $k = 2$. For $\langle N \rangle = 86$, it is 11 % for $k = 1$ and 7 % for $k = 2$. A smaller coherence length increases the contribution of the S_{coh} term. This contribution also depends on the reflection order k, decreasing for higher orders.

For $\langle N \rangle = 86$ and $k = 1$, significant modifications of the profile are observed (Fig. 6, bottom panel). The maxima show small «shoulders» in the inner part of the profiles, as well as the occurrence of a very low-intensity reflection at $h = 0.5$. Similar effects were reported in [4, 9] for even smaller values of $\langle N \rangle$ in an equivalent undoped system. These coherence effects could be misinterpreted as a reduction in crystal symmetry, inhomogeneous chemical composition, or coexistence of a cubic phase from the para-ferroelectric transition.

Therefore, the asymmetries and diffuse intensity in the experimental doublets (Fig. 2) could be influenced not only by domain wall effects but also by coherence between neighboring domains, particularly in PTLa8. To isolate domain wall effects, higher-order reflections ($k \geq 2$) should be used to minimize coherence contributions.

IV.2. Study of the Contribution from Domain Walls with Finite Thickness.

In order to generalize the analysis, the diffracted intensity was evaluated by using equation (2), which includes contributions from the 90° domain walls of finite thickness. For that, it was necessary to estimate the thickness of these walls. Figure 7(a) shows a high-resolution TEM micrograph of PTLa8 with a contrast from two 90° ferroelectric domains. Figure 7(b) shows superimposed electron diffraction patterns from the two domains, with split maxima resulting from their 90° orientation difference.

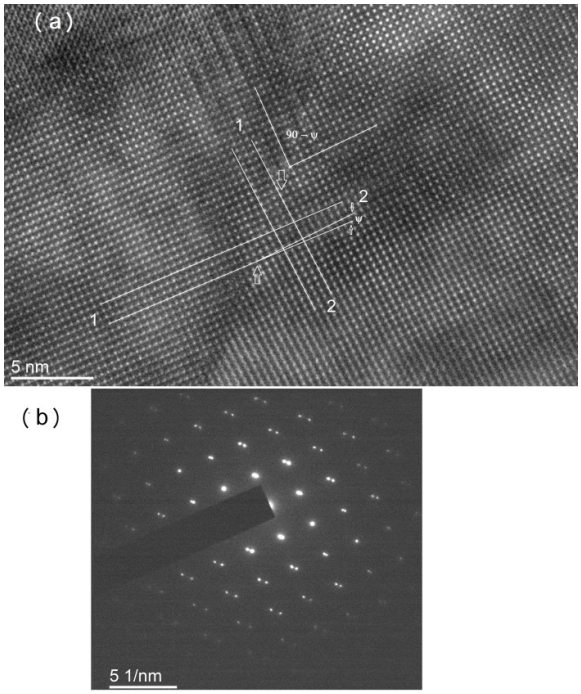

Figure 7. TEM image of sample PTLa8. (a) Contrast associated with a 90° domain wall separating two neighboring ferroelectric domains. (b) Superposition of electron diffraction patterns from the two adjacent domains.

The image was divided into zone 1 (left domain) and zone 2 (right domain). Atomic arrangements deviate at the interface (indicated by arrows), confirming the presence of a thin 90° domain wall between the zones.

The angle between the atomic arrangements of domains 1 and 2 was measured directly from the micrograph. Using $(90° - \psi)$, where $\psi = 2.8°$, it gives 87.2°. This deviation from 90° is necessary to create a coherent twinning interface. The relationship $90° - \psi = 2\arctan(c/a)$ [2] yields $c/a = 1.05$, close to the value of 1.036 determined from XRD for PTLa8.

The difference arises from the nature of the used techniques. Direct measurement of the number of atomic planes in the micrograph (region indicated by arrows in Fig. 7a) estimates the domain wall width to be 3–4 unit cells (approximately 1.2–1.6 nm). This agrees with values reported for other ferroelectric systems. Figures 8 and 9 show the intensity distributions, including coherence effects between adjacent domains (top panels, similar to Figures 5 and 6) and the total intensity calculated for two estimated domain wall widths (2W) in atomic layers.

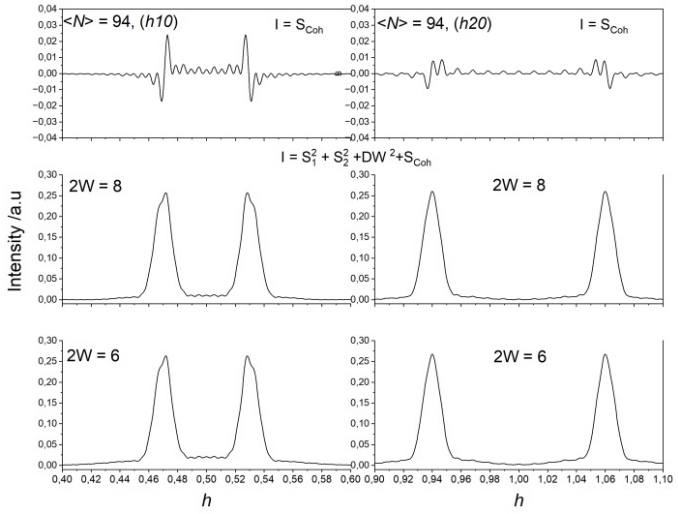

Figure 8. Top panel: Coherence effect between neighboring domains for $\langle N \rangle = 94$ with $k = 1$ and $k = 2$ (as in Fig. 6). Bottom panel: calculation of the total diffracted intensity for the finite wall case, $2W = 8$ and $2W = 6$ atomic layers.

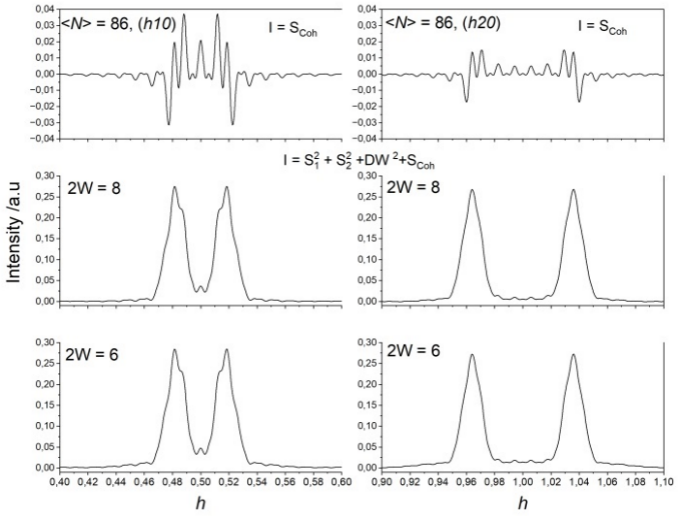

Figure 9. Top panel: Coherence effect between neighboring domains for $\langle N \rangle = 86$ with $k = 1$ and $k = 2$ (as in Fig. 6). Bottom panel: calculation of the total diffracted intensity for the finite wall case, $2W = 8$ and $2W = 6$ atomic layers.

As expected, an increase in background intensity is observed between the doublets, associated with diffuse scattering from the domain wall. This increase is more pronounced for thinner walls. In Fig. 9, the diffuse contribution from the domain wall tends to hide the peak at $h = 0.5$. In experimental patterns, such as that of PTLa8, both effects could contribute to the diffuse background between the doublets. Since coherence effects also contribute to this region, higher-order reflections (e.g., $k = 2$) should be used to explore the domain wall contribution specifically. This result is significant because, in general, the diffuse intensity distribution between pairs of doublets has been associated in the literature only with the effects of the domain walls.

While Figures 5, 6, 8, and 9 show intensity in reciprocal space and Figure 1 shows it in 2θ space for polycrystalline samples, qualitative conclusions can be drawn. The profile shapes in Figure 1, particularly between the doublets, might suggest that domain walls in PTLa8 are narrower on average than in PTDy8. However, PTLa8 also has a smaller $\langle L \rangle$, enhancing coherence effects, especially for $k = 1$. For the (002)/(200) experimental doublet ($k = 2$), the diffuse intensity decreases, likely due to reduced coherence effects at higher orders. Extracting microstructural information from the diffraction profiles in Figure 1 is complex. Peak shape and width are affected not only by coherent domain size and non-uniform microstrains but also by coherence effects and domain wall size. Ignoring these effects can lead to misinterpretation.

V. CONCLUSION

It has been shown that (i) The coherence effects between neighboring ferroelectric domains significantly modify the diffraction profiles, causing asymmetries and contributing to the background between (h00)/(00h) doublets. These effects are more pronounced in samples with smaller domains and for low-order reflections. (ii) 90° domain walls of finite thickness contribute to diffuse background, which increases as the wall width decreases. (iii) The choice of dopant (La^{3+} vs. Dy^{3+}) influences the material's microstructure, affecting domain size and wall density. The results underscore the complexity of the microstructure-property relationship in ferroelectrics and the need for comprehensive analytical approaches for accurate characterization

VI. ACKNOWLEDGEMENT

This work was supported in the framework of an institutional project "Quantitative characterization of the real structure of materials", Program: NAP223LH001-073, and the project PN223LH010-068 from PNCB, Cuba. This work has been also supported by the Brazilian Synchrotron Light Laboratory (LNLS) under the proposal D10B - XPD 10695. Special thanks to Prof. Miran Čeh for the microscopy facilities at the Center for Electron Microscopy and Microanalysis, Jozef Stefan Institute, Ljubljana, Slovenia.

REFERENCES

[1] A. Pramanick, A. D. Prewitt, J. S. Forrester, J. L. Jones, Critical Reviews in Solid State and Materials Sciences **37**, 243 (2012).

[2] N. Floquet, C. M. Valot, M. T. Mesnier, J. C. Niepce, L. Normand, A. Thorel, R. Kilaas, J. Phys. III France **7**, 1105 (1997).

[3] D. R. Taylor, I. P. Swainson, J. Phys.: Condens. Matter **10**, 10207 (1998).
[4] L. Olikhovska, A. Ustinov, F. Bernard, J. C. Niepce, J. Phys. IV France **10**, (2000).
[5] S. A. Hayward, E. K. H. Salje, Z. Kristallogr. **220**, 994 (2005).
[6] H. Boysen, Z. Kristallogr. **220**, 726 (2005).
[7] J. E. Daniels, J. L. Jones, T. R. Finlayson, J. Phys. D: Appl. Phys. **39**, 5294 (2006).
[8] G. Catalan, A. H. G. Vlooswijk, A. Janssens, G. Rispens, S. Redfern, G. Rijnders, D. H. A. Blank, B. Noheda, Integrated Ferroelectrics **92**, 18 (2007).
[9] H. Boysen, J. Phys.: Condens. Matter **19**, 275206 (2007).
[10] B. Khoshnevisan, D. K. Ross, D. P. Broom, M. Babaeipour, J. Phys.: Condens. Matter **14**, 9763 (2002).
[11] Y. U. Wang, Phys. Rev. B **76**, 024108 (2007).
[12] B. Khoshnevisan, Physica C **468**, 2187 (2008).
[13] J. Diao, et al., Phys. Rev. Mater. **4**, 106001 (2020).
[14] Y. Mendez-González, A. Pentón-Madrigal, A. Peláiz-Barranco, S. J. A. Figueroa, L. A. S. de Oliveira, B. Concepción-Rosabal, Physica B **434**, 171 (2014).
[15] A. Peláiz-Barranco, Y. Méndez-González, D. C. Arnold, P. Saint-Grégoire, D. J. Keeble, J. Mater. Sci. **47**, 1094 (2012).
[16] Y. Méndez González, .ªnálisis microestructural y estructural en el sistema ferroeléctrico $PbTiO_3$ dopado con tierras raras", Tesis de maestría, Facultad de Física, Universidad de La Habana, Cuba, (2013).
[17] B. E. Warren, X-ray diffraction, Addison-Wesley (1969).
[18] P. R. Potnis, N.-T. Tsou, J. E. Huber, Materials **4**, 417 (2011).

This work is licensed under the Creative Commons Attribution-NonCommercial 4.0 International (CC BY-NC 4.0, `https://creativecommons.org/licenses/by-nc/4.0`) license.